Chinese Chemical Letters 35 (2024) 109436

Contents lists available at ScienceDirect

Chinese Chemical Letters

journal homepage: www.elsevier.com/locate/cclet

Kinetic study and DFT calculation on the tetracycline abatement by peracetic acid

Dan-Ying Xing[a,b], Xiao-Dan Zhao[a,*], Chuan-Shu He[b,*], Bo Lai[b]

[a] College of Chemical Engineering, Huaqiao University, Xiamen 361021, China
[b] State Key Laboratory of Hydraulics and Mountain River Engineering, College of Architecture and Environment, Sichuan University, Chengdu 610065, China

ARTICLE INFO

Article history:
Received 15 August 2023
Revised 22 November 2023
Accepted 18 December 2023
Available online 22 December 2023

Keywords:
Peracetic acid
Tetracycline
Kinetics
Rate constants
DFT calculation

ABSTRACT

Water contamination by tetracycline (TC) has emerged as an environmental concern owing to its widespread use and antibiotic resistance. Application of peracetic acid (PAA) in the water and wastewater treatment has recently been proposed and demonstrated to be effective for TC abatement, yet the underlying reaction kinetics between the PAA and TC are not yet clear. To explore the reaction kinetics, the effect of solution pH on TC abatement by PAA is studied and the species-specific rate constants are calculated. The ability to donate and accept electrons for different species of TC and PAA is evaluated *via* density functional theory (DFT) calculations. The pH-dependent apparent second-order rate constants of TC abatement by PAA exhibits the parabolic shape with the maximum at pH 8.5 (9.75 L mol^{-1} s^{-1}). This phenomenon is closely related to the speciation of TC and PAA, in which the reaction between PAAH and TTC^{2-} possesses the highest species-specific rate constants according to the kinetic simulation. Further DFT calculations suggest that the HOMO of $TTCH^{+}$, TTC, TTC^{-}, TTC^{2-} and the LUMO of PAAH and PAA^{-} are −6.40, −6.26, −5.10, −4.94 eV and −0.24, 0.60 eV, respectively. According to the DFT calculations, deprotonation of TC and PAA leads to an increase of the HOMO value of TC and the LUMO value of PAA. Furthermore, the $HOMO_{TC}$–$LUMO_{PAA}$ values is in good agreement with the trend of species-specific rate constants, which can be used to evaluate the reactivity between PAA and TC with different species. This study provides the kinetic data and theoretical basis for the reaction of PAA and TC, which is critical for the application of PAA in the treatment of water and wastewater.

Tetracycline antibiotics (TCs) are a class of broad-spectrum antibiotics produced by actinomycetes, mainly containing tetracycline (TC), oxytetracycline (OTC) and chlortetracycline (CTC) with a tetraphenyl basic skeleton [1]. TCs are widely used in the medical and animal husbandry industries due to their excellent antimicrobial properties and cost-effectiveness [2,3]. However, metabolism of TCs at low levels in organisms can result in their release into the aquatic environments as parent compounds (>75%) and the concomitant high detection frequencies and concentrations in water. As one of the most widely used TCs, TC has been detected in wastewater, surface water and groundwater at concentrations of 2.2 mg/L, 0.1 μg/L and 4.5 μg/L, respectively [4]. Low concentrations of TC can lead to cytotoxicity and genetic resistance, threatening the ecosystem and human health [5,6]. In particular, the frequent detection of TC in medical wastewater may lead to bacterial resistance with potential harm to ecosystems [7]. Therefore, it is of significance to study the effective technologies for rapid TC abatement.

Peracetic acid (PAA), generated *via* the reaction between acetic acid and H_2O_2 (Eq. S1 in Supporting information), has been widely used as the antibacterial agent and disinfectant after it was first synthesized in 1902 [8–10]. Compared to conventional chlorine disinfectants, PAA has comparable disinfection reaction activity and does not require dichlorination in the subsequent process [11,12]. The United States Environmental Protection Agency has approved the application of PAA disinfection for the treatment of sewage overflows in 1999 and for wastewater treatment in 2012 [12,13]. As a result, PAA is widely used in wastewater treatment, disinfection, medical, chemical and paper industries [8,14]. The excellent performance of PAA in disinfection application (especially in hospital wastewater disinfection) provides a good basis for its use in the chemical oxidation for the pollutant abatement.

The degradation of pollutants is often achieved using advanced oxidation process that activate PAA to generate free radicals [13,15,16], ignoring the oxidative properties of PAA itself. Compared with conventional oxidants, PAA possesses higher stan-

* Corresponding authors.
E-mail addresses: zhaoxd_1987@163.com (X.-D. Zhao), hecs@scu.edu.cn (C.-S. He).

https://doi.org/10.1016/j.cclet.2023.109436
1001-8417/

dard oxidation potential (E^0 =1.96 V) and therefore can selectively oxidize organic pollutants with specific structures in wastewater [12,17,18]. For instance, Zhang *et al.* and Du *et al.* found that PAA can attack the sulfur group of β-lactam and amino acids for its rapid oxidative degradation [19,20]. In addition, Kim and Huang summarized the ability of PAA to oxidize 123 organic compounds found that the rate constants of PAA with the compounds varied by about ten orders of magnitude [21], which is lower than O_3 [22], HOCl [23], but close to Fe(VI) [24]. Therefore, the reaction rate of PAA with organic contaminant greatly depends on the structure of the contaminant.

Regarding that PAA is an electrophilic reagent and TC contains several electron-rich fractions, TC is expected to exhibit considerable reactivity toward PAA [21,25]. A previous study has demonstrated the reactivity between PAA and TC, yet the species-specific reactions for the reaction of PAA and TC are not clear, and the electron-donating and electron-accepting properties of the different species of TC and PAA needs to be elucidated. At the same time, the research method of combining experimental results with density functional theory (DFT) calculations, which can provide in-depth information with respect to the molecular level [26–29]. Is there a link between species-specific rate constants and the DFT calculations for the ability to gain or lose electrons of different TC and PAA species? Most importantly, considering that PAA is a commonly used oxidant in the disinfection of hospital wastewater and the frequent detection of TC in medical wastewater, oxidative of TC by PAA is practically feasible.

Therefore, the objectives of this work are: (i) To evaluate the efficacy of oxidative abatement of TC by PAA for different pH conditions; (ii) to construct the kinetic model and calculate the species-specific reaction rate constants for the reaction between PAA with TC; (iii) to analyze the electron-donating and accepting property *via* the calculation of the highest occupied molecular orbital (HOMO), lowest unoccupied molecular orbital (LUMO), HOMO−LUMO gap, and electrostatic potential of TC and PAA in different forms based on DFT and (iv) to identify the discrepancy of the reactive sites *via* the Fukui functions for different TC species.

The detail information of chemicals was shown in the Text S1 in Supporting information.

The batch experiments of TC abatement were performed in 250 mL glass vessel with 200 mL reaction solution and the rotary speed of 500 rpm. The experimental temperature was controlled at 25 °C using the water bath. The 10 mmol/L acetate buffer (3.5 < pH < 5), phosphate buffer (5 < pH < 8), borate buffer (pH > 8) or adding pre-calculated amounts of H_2SO_4 (3.0 ≤ pH < 3.5) were used to maintain the pH of the solution. TC was added in advance to the glass, followed by the addition of PAA concentration 10 times or higher than the initial TC concentration to initiate the reaction. The sample with 1 mL was withdrawn using the pipette gun at predetermined time intervals and subsequently added to the liquid phase vials containing 100 μL $Na_2S_2O_4$ (100 mmol/L) for TC concentration analysis. All experiments were repeated at least three time to minimize standard deviation.

The methods of determination the PAA and H_2O_2 concentration in the PAA stock solution were shown in the Text S2 (Supporting information). The details of analytical methods and DFT calculation were provided in the Text S3 (Supporting information).

Fig. S1 (Supporting information) presents TC abatement as a function of time by PAA under neutral conditions. TC does not undergo self-attenuation reaction, exhibiting stable properties. In the presence of 200 μmol/L PAA, rapid removal of TC (72.9%) is achieved within 60 min of reaction, and CH_3COOH and different concentrations of H_2O_2 in PAA solution exert negligible effect on the degradation of TC (Fig. S2 in Supporting information), indicating the redox reaction between the PAA and TC at pH 7.0. Comparison of kinetic data for the oxidation of TC by typical oxidants is shown in Table S1 (Supporting information). High TC abatement efficiencies can be achieved at low PAA concentrations, while the reaction between the PAA and TC is milder and reduces the generation of chlorine-containing by-products compared to chlorine oxidizers. To further explore the effect of pH, TC abatement is monitored under different pH conditions *via* controlling the ratio of PAA:TC. The specific experimental conditions are shown in Table S2 (Supporting information) (Fig. 1a). The difference in PAA concentration at different pH conditions is mainly for more accurate calculation of k_{obs}. The pH of the solution remains constant during the reaction (Fig. S3 in Supporting information). Subsequently, TC abatement by PAA is plotted by *pseudo*-first-order kinetics with high linear correlation coefficients (Fig. S4a in Supporting information) and then the *pseudo*-first-order rate constants (k_{obs}) of TC abatement are calculated (Fig. S4b in Supporting information). The TC abatement at different PAA concentrations follows pseudo-first-order kinetics (Eq. 1, Figs. S5a and b in Supporting information). The k_{obs} of TC abatement increases linearly with increasing PAA concentration. The ln k_{obs} *vs.* ln C_{PAA} plot presents a linear relationship with the slope close to 1, indicating that k_{obs} with PAA concentration is the first-order [25]. Therefore, the reactions of PAA and TC can be described in terms of second-order kinetics (Eq. 2). The apparent second-order rate constants ($k_{2,app}$) are determined in the pH range of 3.0−11.0 (Fig. 1b). As can be seen, TC abatement under alkaline conditions is more efficient than under acidic conditions. This is mainly due to the increased deprotonation of TC under alkaline conditions, where the electron density of deprotonated TC is higher than that of protonated TC, thus facilitating the attack of PAA [30]. However, as the pH continues to increase, the proportion of deprotonated PAA is the dominant species, leading to the decrease in its ability to TC oxidation, which is consistent with a previous report [25]. The decay of PAA with time at different pH is also determined in the presence and absence of TC (Figs. S6a and b in Supporting information). The PAA decay can be negligible (<10%) under acidic to weakly basic conditions. However, at pH 10.0 and 11.0, the PAA decay exceeds 10%, which is mainly due to the self-decaying reaction of PAA under high pH conditions (Eqs. 3−5) [31,32].

$$-\frac{d[TC]}{dt}=k_{obs} \times [TC] \quad (1)$$

$$-\frac{d[TC]}{dt}=k_{2,app} \times [TC] \times [PAA] \quad (2)$$

$$CH_3C(O)OOH + H_2O \leftrightarrow CH_3C(O)OO^- + H_3O^+,\ pK_a = 8.2 \quad (3)$$

$$CH_3C(O)OO^- + CH_3C(O)OOH \rightarrow CH_3COOH + CH_3COO^- + O_2 \quad (4)$$

$$CH_3C(O)OO^- + H_2O_2 \rightarrow CH_3COO^- + H_2O + O_2 \quad (5)$$

The reaction between PAA and TC can be expressed as a bimolecular reaction, which is closely related to their respective speciation (Figs. 2a and b) [33,34]. As illustrated in Fig. 1b, the $k_{2,app}$ values of TC by PAA exhibits strong pH-dependency. $k_{2,app}$ increases with increasing pH with the maximum around pH 8.5, and decreases rapidly when pH is further increased. The strong pH-dependency of $k_{2,app}$ is due to the fact that PAA and TC have different species with different reactivities. Therefore, the species-specific kinetic model for the reaction of PAA and TC is constructed based on the equations listed in Table 1. TC has three pK_a-values (pK_{a1} 3.32, pK_{a2} 7.78 and pK_{a3} 9.58) corresponding to four different species, *i.e.,* TTC^+ (with one positive charge), TTC (neutral), TTC^- (with one negative charge) and TTC^{2-} (with two negative charge)

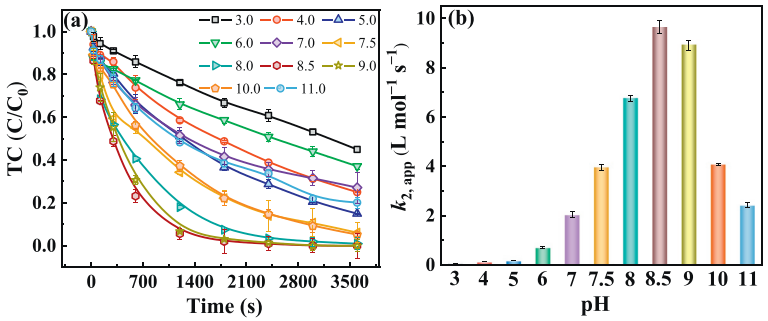

Fig. 1. (a) TC oxidation abatement by PAA under different pH. (b) The $k_{2,app}$ of TC abatement under different pH. Experimental conditions: [PAA] = 200–3000 μmol/L, [TC] = 20 μmol/L, pH 3.0–11.0.

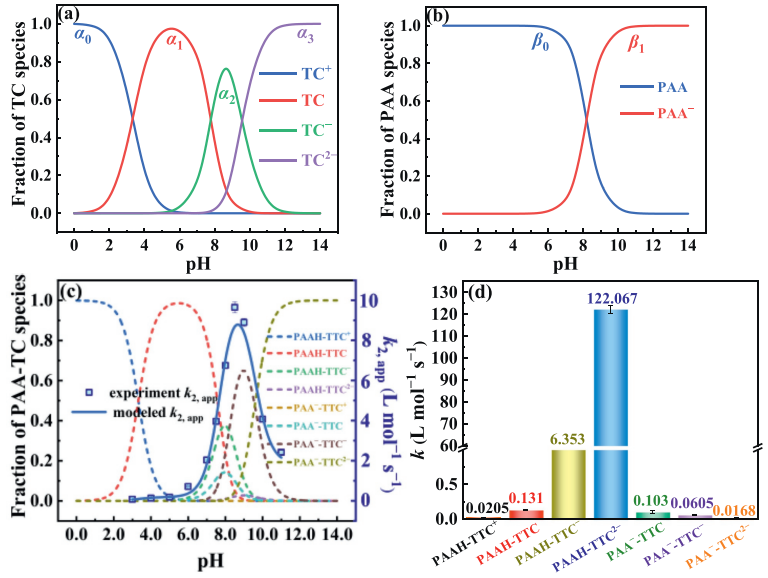

Fig. 2. (a) TC speciation as a function of pH. (b) PAA speciation as a function of pH. (c) Effect of pH on the PAA-TC species ($\beta_j \times \alpha_i$) and kinetic modeling for the $k_{2,app}$ of TC with PAA. (d) Species-specific reaction rate constants for PAA with TC. Experimental conditions: [PAA] = 200–3000 μmol/L, [TC] = 20 μmol/L, pH 3.0–11.0.

Table 1
Kinetic modeling equations.

Eqs.	Number
$-\frac{d[TC]}{dt} = k_{obs} \times [TC]$	(1)
$-\frac{d[TC]}{dt} = k_{2,app} \times [TC] \times [PAA]$	(2)
$[TC]_{Total} = [TTC^+] + [TTC] + [TTC^-] + [TTC^{2-}] = a_i \times [TC]_{Total}$	(6)
$a_0 = (1 + \frac{K_{a1}}{[H^+]} + \frac{K_{a1}K_{a2}}{[H^+]^2} + \frac{K_{a1}K_{a2}K_{a3}}{[H^+]^3})^{-1}$	(7)
$a_1 = (\frac{[H^+]}{K_{a1}} + 1 + \frac{K_{a2}}{[H^+]} + \frac{K_{a2}K_{a3}}{[H^+]^2})^{-1}$	(8)
$a_2 = (\frac{[H^+]^2}{K_{a1}K_{a2}} + \frac{[H^+]}{K_{a2}} + 1 + \frac{K_{a3}}{[H^+]})^{-1}$	(9)
$a_3 = (\frac{[H^+]^3}{K_{a1}K_{a2}K_{a3}} + \frac{[H^+]^2}{K_{a2}K_{a3}} + \frac{[H^+]}{K_{a3}} + 1)^{-1}$	(10)
$[PAA]_{Total} = [PAAH] + [PAA^-] = \beta_j \times [PAA]_{Total}$	(11)
$\beta_0 = (1 + \frac{K_a}{[H^+]})^{-1}$	(12)
$\beta_1 = (\frac{[H^+]}{K_a} + 1)^{-1}$	(13)
$-\frac{d[TC]_t}{dt} = k_{2,app} \times [TC]_t \times [PAA]_t = \sum_{i,j}^{m,n} k_{i,j} \times a_i \times \beta_j \times [TC]_t \times [PAA]_t$	(14)
$k_{2,app} = \sum_{i,j}^{m,n} k_{i,j} \times a_i \times \beta_j$	(15)

Where i = 0, 1, 2 and 3, and a_0, a_1, a_2, a_3 represent the distribution coefficients of TTC^+, TTC, TTC^-, TTC^{2-}, respectively.
Where j = 0, 1, and β_0, β_1 represent the distribution coefficients of PAAH, PAA^-, respectively.

(Fig. S7a in Supporting information). The amount of each component of TC at all pH conditions can be calculated by the Eqs. 6–10, which is displayed in Fig. 2a. Similarly, PAA with a pK_a value at pH 8.2 (Fig. S7b in Supporting information) possesses two species, protonated PAAH and deprotonated PAA^-. The content of PAA at different pH can be expressed by Eqs. 11–13 and Fig. 2b. Then, substituting Eq. 6 and Eq. 11 into Eq. 2, and yields Eq. 14 and Eq. 15. $k_{i,j}$ denotes the species-specific second-order rate constant between the i species of TC and the j species of PAA. The molar fractions of the different species of PAA and TC at different pH are obtained by $a_i \times \beta_j$, as illustrated in Fig. 2c.

Based on the above analysis, the value of $k_{i,j}$ is obtained by least squares regression of the experimental $k_{2,app}$ with Eq. 15 *via* the user-defined nonlinear regression equation in the Origin software and the fitted curve is shown in Fig. 2c. The experimental $k_{2,app}$ and modeled $k_{2,app}$ can be well fitted and the species-specific rate constants can be correspondingly calculated, as shown in Fig. 2d. In the fitted data, the reaction rate constant between PAA^- and TTC^+ is 0. At the same time, the mole fraction of PAA^- and TTC^+ is extremely low (Fig. 2c), so the reaction between PAA^- and TTC^+ can be negligible in the overall reaction. The reaction of protonated PAAH to each species of TC is significantly higher than that of the deprotonated PAA^-. Especially, the species-specific reaction of PAAH with TTC^{2-} is significantly higher than that of the other species, which mainly contributes to the reaction between PAA and TC. For different TC species, the reactivity of PAA follows an order of TTC^{2-} > TTC^- > TTC. This is mainly because the higher deprotonation of TC means the higher electron density of ring structure. Interestingly, the reactivity between PAA^- and each species of TC is opposite to PAAH. This is mainly due to the electrostatic repulsion between the negative charge of deprotonated PAA^- and that of deprotonated TC, which results in a decrease in their reactivity.

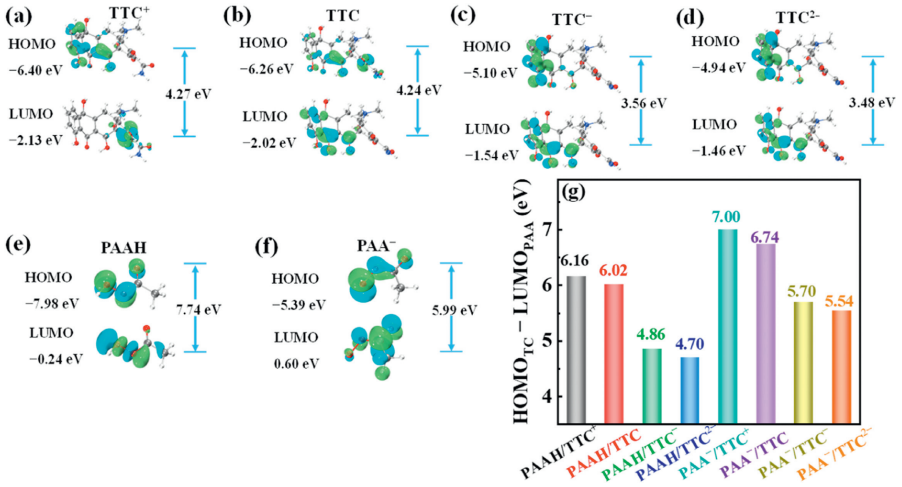

Fig. 3. The HOMO, LUMO and HOMO–LUMO gap of (a) TC^{+}; (b) TC; (c) TC^{-}; (d) TC^{2-}; (e) PAA; (f) PAA^{-}; (g) $HOMO_{TC}$–$LUMO_{PAA}$ gap.

As mentioned earlier, the differences in the PAA and TC reaction rates of different species are due to differences in their ability to gain and lose electrons. In DFT calculations, the frontier orbital theory can reflect the ability of a molecule to gain or lose electrons ability of [35,36]. In a molecule, the electron on HOMO has the highest energy and is the least bound, which is the most active and easy to lose electrons. In comparison, LUMO has the lowest energy of all the unoccupied orbitals and is the easiest to accept electrons. These two orbitals determine the electron gain/loss and transfer ability of the molecule. Therefore, the frontier orbital theory is performed to further understand the electron gaining and losing abilities of different species of PAA and TC. Higher HOMO means the higher ability to lose electrons and tendency for oxidation and lower LUMO means the higher ability to gain electrons and tendency for reduction. In comparison, the HOMO–LUMO gap is the energy difference between HOMO and LUMO. A smaller HOMO–LUMO gap indicates lower energy required to transfer an electron from HOMO to LUMO and more reactive molecule, which promotes the occurrence of chemical reactions. The molecules with a large HOMO–LUMO gap tend to be more stable because the electron leaps are less likely due to the higher energy barrier [32]. The HOMO, LUMO and HOMO–LUMO gap of TTC^{+}, TTC, TTC^{-}, TTC^{2-}, PAAH and PAA^{-} are calculated, as shown in Fig. 3. In terms of TC, the HOMO values of TTC^{+}, TTC, TTC^{-}, TTC^{2-} are –6.40 eV, –6.26 eV, –5.10 eV, –4.94 eV, respectively. The electron-losing capacity of TC increases with increasing deprotonation. For PAA, the LUMO values of PAAH and PAA^{-} are –0.24 eV and 0.60 eV, respectively. The electron-gaining capacity of PAA increases with increasing protonation. Meanwhile, the HOMO–LUMO gap of the four states of TC are 4.27 eV, 4.24 eV, 3.56 eV and 3.48 eV, representing that TC deprotonation can significantly facilitate the electrophilic attack by PAA, and in particular the HOMO–LUMO gap of TTC^{-} and TTC^{2-} are much smaller than TTC^{+} and TTC, which corresponds to the rate constants of the reaction.

Previous studies have reported that the energy of HOMO–LUMO gap between two molecules can be used to evaluate their reactivity [37,38]. The smaller HOMO–LUMO gap indicates the larger polarizability, reflecting the excitation energy. In this study, the reactivity between different species of PAA and TC is evaluated to use the HOMO of different TC species minus the LUMO of different PAA species. As shown in Fig. 3g, the $HOMO_{TC}$–$LUMO_{PAA}$ values are observed to follow an order of decreased by increasing deprotonation of TC and increased by protonation of PAA, which is in good agreement with the trend of species-specific rate constants (Fig. 2d). In fact, when the species-specific rate constant is calculated

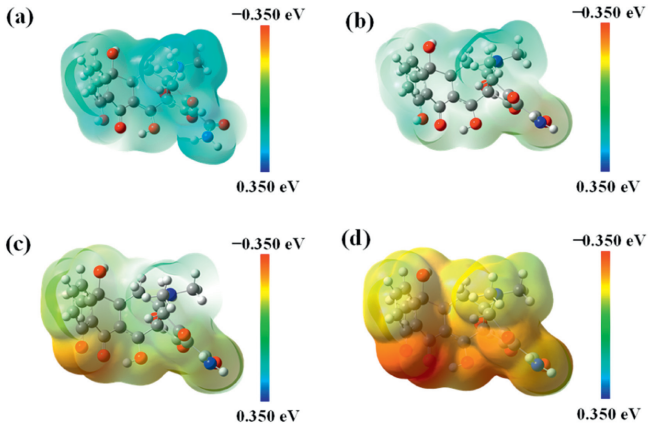

Fig. 4. The ESP of (a) TC^{+}; (b) TC; (c) TC^{-}; (d) TC^{2-}.

by experimental means, the electrostatic repulsion may exist when PAA and TC molecules in different states. However, in the defining $HOMO_{TC}$–$LUMO_{PAA}$, only the theoretical HOMO and LUMO of TC and PAA are taken into account, and the electrostatic repulsion present in PAA and TC is not taken into account when $HOMO_{TC}$–$LUMO_{PAA}$ value is related to the actual species-specific reaction rate constants. Therefore, disregarding the effect of electrostatic interactions, the smaller $HOMO_{TC}$–$LUMO_{PAA}$ value is, the bigger species-specific rate constant will be. Furthermore, the degree of deprotonation of TC significantly affects the $HOMO_{TC}$–$LUMO_{PAA}$ gap. Similarly, the deprotonation of PAA leads to an increase of the $HOMO_{TC}$–$LUMO_{PAA}$ gap with different species of TC. The smaller energy level of $HOMO_{TC}$–$LUMO_{PAA}$ suggests the higher reactivity and the correspondingly larger reaction rate constants.

The deprotonation of TC changes its electricity and affects its electron arrangement. Thus, the electrostatic potential (ESP) of TC is calculated, as shown in Fig. 4. Deprotonation of TC significantly affects its electron arrangement, potentially influencing the site at which its electrophilic reactions occur. In general, PAA is more inclined to electrophilic attack on the electron-rich sites of organic pollutants, and in particular, shows high reactivity towards the N-containing groups of phenolic compounds [21,25]. TC containing N groups and phenolic groups (Fig. S8 in Supporting information) possesses the four-rings structure and different degrees of protonation may alter their electron arrangement. The electrophilicity index f^{-} in the Fukui function can more accurately describe the electron-donating and accepting property on the atom. Therefore,

the Fukui functions for TTC^{+}, TTC, TTC^{-} and TTC^{2-} are calculated, as shown in Fig. S9 (Supporting information) and Tables S3−S6 (Supporting information), and the atomic numbers are shown in Fig. S10 (Supporting information). The easily attacked sites of four TC species are located at the carbon sites of the B and C rings, which is consistent with previous studies that TC are more susceptible to hydrogenation and hydroxylation reactions at the carbon sites [7,25]. Moreover, the sites susceptible to attack for different TC species is hardly changed, and thus the degree of deprotonation of TC does not affect its susceptibility to be attacked. Therefore, the protonation and deprotonation of TC does not change its oxidation products by PAA.

In this work, the kinetics for the reaction between TC and PAA is explored, and the reactivity between different TC species and PAA is qualitatively evaluated by DFT calculations. The reactivity of PAA and TC is highly pH-dependent. Reactions of PAAH and TTC^{2-} are major contributors to reactions between PAA and TC. Electron-donating capacity of TC and electron-acquiring capacity of PAA exhibits a significant variation with increasing deprotonation level, which is proved by DFT calculations. The protonation of TC does not affect the reactive sites. Compared to conventional oxidizing agents, lower concentrations of PAA are required to achieve efficient TC degradation and no chlorine-containing by-products are produced. Hence, PAA oxidation exhibits significant advantages of the strong oxidizing ability of protonated PAA for TC abatement and the application prospects in wastewater treatment.

Declaration of competing interest

The authors declare that they have no known competing financial interests or personal relationships that could have appeared to influence the work reported in this paper.

Acknowledgments

The authors wish to thank the National Natural Science Foundation of China (No. 52170088), Natural Science Foundation of Fujian Province (No. 2022J05064) and the Fundamental Research Funds for the Central Universities (No. ZQN-1118).

Supplementary materials

Supplementary material associated with this article can be found, in the online version, at doi:10.1016/j.cclet.2023.109436.

References

[1] L. Xu, H. Zhang, P. Xiong, et al., Sci. Total Environ. 753 (2021) 141975.
[2] T. Wang, J. He, J. Lu, et al., Chin. Chem. Lett. 33 (2022) 3585–3593.
[3] S. Li, Y Yang, H Zheng, et al., Water Res. 225 (2022) 119176.
[4] M. Xu, J. Deng, A. Cai, et al., Chem. Eng. J. 384 (2020) 123320.
[5] S.Y. Yu, Z.H. Xie, X.Y. Wu, et al., Chin. Chem. Lett. 35 (2024) 108714.
[6] F. Sun, X. Yang, F. Shao, et al., Chin. Chem. Lett. 34 (2023) 108563.
[7] J. Chen, J. Xu, T. Liu, et al., J. Hazard. Mater. 386 (2020) 121656.
[8] W.P. da Silva, T.D. Carlos, G.S. Cavallini, et al., Water Res. 168 (2020) 115143.
[9] Z.H. Xie, C.S. He, Y.L. He, et al., Water Res. 232 (2023) 119666.
[10] S.R. Yang, Z.H. Liang, Y. Wen, et al., ACS ES&T Eng. 3 (2023) 271–282.
[11] K. Zhang, X. Zhou, P. Du, et al., Water Res. 123 (2017) 153–161.
[12] X.W. Ao, J. Eloranta, C.H. Huang, et al., Water Res. 188 (2021) 116479.
[13] H. Cao, Y.H. Dai, L.L. Wu, et al., Sep. Purif. Technol. 319 (2023) 124083.
[14] C. Neus, D.F. Cecilia, M. Roberta, et al., Water Res. 169 (2020) 115227.
[15] Y.H. Dai, C.D. Qi, H. Cao, et al., Sep. Purif. Technol. 288 (2022) 120716.
[16] Y.H. Dai, H. Cao, C.D. Qi, et al., Chem. Eng. J. 451 (2023) 138588.
[17] T. Luukkonen, S.O. Pehkonen, Crit. Rev. Env. Sci. Tec. 47 (2017) 1–39.
[18] M.F. He, W.Q. Li, Z.H. Xie, et al., Water Res. 222 (2022) 118887.
[19] Z. Yuan, Y. Ni, A.R.P. Van Heiningen, Can. J. Chem. Eng. 75 (1997) 37–41.
[20] P.H. Du, W. Liu, H.B. Cao, et al., Water Res. X 1 (2018) 100002.
[21] J. Kim, C.H. Huang, ACS ES&T Water 1 (2021) 15–33.
[22] U. von Gunten, Water Res. 37 (2003) 1443–1467.
[23] D. Marie, U. von Gunten, Water Res. 42 (2008) 13–51.
[24] Y.H. Lee, S.G. Zimmermann, A.T. Kieu, et al., Env. Sci. Tec. 43 (10) (2009) 3831–3838.
[25] J. Chen, J. Xu, T. Liu, et al., Chem. Eng. J. 431 (2022) 134190.
[26] S.X. He, E.Y. Wu, M.J. Shen, et al., ACS ES&T Eng. 3 (2023) 651–660.
[27] S. Gao, H.D. Ji, P. Yang, et al., Small 19 (2022) 202206114.
[28] Y. Liu, L. Chen, X.N. Liu, et al., Chin. Chem. Lett. 33 (2022) 1385–1389.
[29] X.C. Zeng, J.F. Zhu, G.H. Zhang, et al., Chem. Eng. J. 468 (2023) 143536.
[30] Y.Y. Chen, Y.L. Ma, J. Yang, et al., Chem. Eng. J. 307 (2017) 15–23.
[31] Z.P. Wang, J.W. Wang, B. Xiong, et al., Environ. Sci. Technol. 54 (2019) 464–475.
[32] D.Y. Xing, S.J. Shao, Y.Y. Yang, et al., Water Res. 222 (2022) 118930.
[33] A. Karlesa, G.A.D. De Vera, M.C. Dodd, et al., Environ. Sci. Technol. 48 (2014) 10380–10389.
[34] C. Zhao, L.E. Arroyo-MORA, A.P. DeCaprio, et al., Water Res. 233 (2023) 119773.
[35] K. Fukui, T. Yonezawa, H. Shingu, J. Chem. Phys. 20 (2004) 722–725.
[36] K. Fukui, T. Yonezawa, C. Nagata, et al., J. Chem. Phys. 22 (2004) 1433–1442.
[37] R. Zhang, X. Wang, L. Zhou, et al., Water Res. 135 (2018) 144–154.
[38] A. Asghar, M.M. Bello, A.A.A. Raman, et al., Heliyon 5 (2019) e02396.